RSC Advances

ROYAL SOCIETY OF CHEMISTRY

www.rsc.org/advances

RSC Advances

ARTICLE

Facile Solvothermal Synthesis of Ag/Fe_3O_4 Nanocomposites and Their SERS Applications in On-line Monitoring of Pesticide Contaminated Water

Received 00th January 20xx,
Accepted 00th January 20xx

DOI: 10.1039/x0xx00000x

www.rsc.org/

Yufeng Shan,[a,b] Yong Yang,[*a,b] Yanqin Cao,[a,b] and Zhengren Huang[a,b]

The nanocomposites of noble metal and magnetic material deliver both SERS activity and magnetic property, and thereby have great advantages over trace analysis in the field of analytical chemistry, biological and environmental sciences. In this work, Ag/Fe_3O_4 nanocomposites have been obtained by a facile one-pot solvothermal method. The Fe_3O_4 nanoparticles (NPs) compounded with Ag possess excellent superparamagnetism, which guarantees an effective self-aggregation of Ag/Fe_3O_4 composites. The saturation magnetic moment and SERS activity of as-prepared nanocomposites are easily optimized by adjusting the mole ratio of silver oleate and iron oleate. The sample with Ag/Fe = 5 possesses optimal SERS performance for both R6G and MB detection. The Fe_3O_4 NPs with ultra small size behave just like glue or contractile net which would wrap the Ag NPs together under external magnetic field and give rise to high-density and high-intensity "hot-spots". The enhancement factors (EFs) of sample with Ag/Fe = 5 are over ~ 10^8 both for R6G and MB detection. The as-prepared magnetic nanocomposites have been applied to realize an efficient but convenient real-time on-line monitoring of atrazine in flowing pesticide contaminated water, which show enormous potential in the application of on-line monitoring for industrial and agricultural production.

Introduction

Surface enhanced Raman scattering (SERS) has inspired researchers' great interest for decades on account of its prominent applications in many fields, such as biological sensing, environmental monitoring, archaeology and criminal investigation.[1-10] Benefiting from the enormous surface plasmon resonance (SPR) effect,[11] the metal nanostructures (mainly Au and Ag) are commonly used as active-SERS substrates to realize ultrasensitive, rapid and nondestructive analysis, detection and imaging. For metal-based SERS substrates, it is well-known that in most cases, electromagnetic (EM) enhancement acts as the dominant contributor to an excellent SERS performance. A remarkable EM enhancement is mainly ascribed to the construction of "hot-spots" in the aggregated metal nanostructures.[12,13] There are several simple but effective methods to realize the beneficial aggregation of Ag or Au NPs, such as salt caused aggregation effect,[14-16] dynamic solvent volatilization,[17] magnetic induced aggregation,[18-22] and so on. Among them, the combination of noble metals and magnetic materials applied as SERS substrates has undoubtedly drawn more attention due to the excellent magnetic, non-toxic, and biocompatible properties of magnetic nanomaterials.[23-27] By introducing the magnetic component, the embarrassment in separation and concentration of target products is also well avoided, and more importantly, magnetic component could bring abundant "hot-spots" by an effective magnetic-induced aggregation.

So far, Ag/Fe_3O_4 nanocomposites used as SERS substrates have been widely reported.[18, 28-34] Notably, a two-step method is preferred in literature to prepare unique core-shell (Fe_3O_4@Ag or Ag@Fe_3O_4) composite structures.[24, 33, 35-38] However, the enclosing structure would excessively hinder the function of those encapsulated in the shell, that is, weakening the magnetism of Fe_3O_4 or SPR effect of Ag NPs. Moreover, even for recently developed one-step synthetic methodology, Fe_3O_4 NPs are actually more prone to grow on Ag crystals owing to the lattice match, and impede the effective adsorption of analyte molecules on "hot-spots", which is detrimental to the SERS activity.[32, 34]

Besides, the content of Fe_3O_4 in composite substrates also has a marked impact on the SERS activity. It should be noted that although a high content of Fe_3O_4 in composite SERS substrate would give a fast magnetic response, Fe_3O_4 itself does not show any SERS activity, and excessive Fe_3O_4 component would do harm to the overall SERS property.[29, 32] However, a low content of Fe_3O_4, in general, is

[a] State Key Laboratory of High Performance Ceramics and Superfine Microstructures, Shanghai Institute of Ceramics, Chinese Academy of Sciences, 1295 Dingxi Road, Shanghai 200050, China. Fax: +86-21-52414219; Tel: +86-21-52414321; E-mail: yangyong@mail.sic.ac.cn
[b] Graduate School of the Chinese Academy of Sciences, Beijing, China.

† Electronic Supplementary Information (ESI) available: [diagram of the composite SERS substrate, magnified low field magnetic hysteresis loops, Raman spectra for the calculation of EF, TEM image of Ag NPs wrapped by glue-like Fe_3O_4 and schematic diagram of the "glue-like" Fe_3O_4 NPs, a table for XPS results, and the detailed EF calculation method.]. See DOI: 10.1039/x0xx00000x

hardly to guarantee an effective aggregation of Ag NPs. To achieve a good aggregation of Ag NPs with as low content Fe_3O_4 as possible, small sized Fe_3O_4 with excellent superparamagnetism is expected.

Nowdays, an increasing number of aqueous pollutants are threatening the world's ecosystem and human-health. Taking China for example, every year more than 1,700 water pollution accidents have happened, and hundreds of millions of people are facing serious health hazards from unsafe drinking water. To better solve such problems, besides timely wastewater treatment, it makes more sense to prevent and control the effluent discharge from source. Therefore, rapid pollutant recognition from the wastewater in the blow-off pipe from the factories is vitally important for effective monitoring and control of the pollution source. Accordingly, a good design of on-line monitoring system that helps to prevent the excess pollutants discharge at source is in urgent need. However, as far as we know, a reliable, effective and controllable on-line monitoring device is still extremely absent. So we anticipate this dual-functional composite SERS substrates could exhibit more abilities in on-line monitoring of sewage discharge.

In this work, a facile, low cost, and efficient one-pot solvothermal method was developed to prepare Ag/Fe_3O_4 nanocomposites, in which homemade organic precursors of silver oleate and iron oleate were applied as metallic ion sources. The as-prepared Ag/Fe_3O_4 composites deliver a unique structure that Ag NPs are just attached to the "glue-like" Fe_3O_4 colloids. The magnetic "glue" composed of plenty of small sized Fe_3O_4 NPs exhibit excellent superparamagnetism, which is of great concern for the magnetism-induced aggregation of Ag NPs. In order to seek the optimized SERS substrate, a series of various compositions of Ag/Fe_3O_4 were prepared by altering the Ag/Fe mole ratios. Finally, the optimized Ag/Fe_3O_4 SERS substrates were further used to realize a real-time on-line monitoring device for the first time. By utilizing this on-line monitoring device, pesticide in the flowing solution has been successfully detected. This strategy that utilizes magnetic hybrid SERS substrate for the controllable on-line pollution monitoring could do more help for safer industrial and agricultural production.

Experimental section

Materials and Instruments

Ferric nitrate nonahydrate ($Fe(NO_3)_3{\cdot}9H_2O$), silver nitrate ($AgNO_3$), oleic acid, octadecylene, sodium hydrate (NaOH), rhodamine 6G (R6G), methyl blue (MB) and atrazine were purchased from Aladdin Co., Ltd. All reagents are analytically pure and used as received without further purification.

Transmission electron microscopy (TEM) and high resolution TEM (HRTEM) images were obtained on a JEOL JEM-2100F field emission source transmission electron microscope with an accelerating voltage of 200 kV. UV-Vis diffuse reflectance spectra were recorded on a PE lambda 950 instrument. X-ray photoelectron spectroscopy (XPS) spectra were collected on a Leybold MAX 200 photoelectron spectrometer equipped with an Mg Kα radiation source (1253.6 eV) operated at 200 W. The magnetic performance was conducted by a Physical Property Measurement System (PPMS, Quantum Design Company). SERS spectra were collected on a Nanofinder 30 (TII Tokyo Instruments, Inc) and all spectra were taken at room temperature excited by a solid state laser (λ = 532 nm) with the laser excitation power 0.025 mW for rhodamine 6G (R6G) detection, 0.065 mW for methyl blue (MB) detection and 0.1 mW for atrazine detection. Calibration was conducted by the Raman shift of single crystal silicon at 520.4 cm^{-1} and a 600 g/mm grating was equipment to disperse the signal to generate a spectra resolution of ~2.88 cm^{-1}.

Preparation of silver oleate and iron oleate precursors

Metal fatty acid salts were prepared according to the published procedures.[39] Taking iron oleate for example, 12 mmol $Fe(NO_3)_3{\cdot}9H_2O$ was dissolved in 80 ml methanol, and then 36 mmol (12 ml) oleic acid was added into the solution. 36 mmol NaOH dissolved in 80 ml methanol was further slowly dropped in the mixture with vigorous magnetic stirring. The final suspension was stirred overnight to ensure a complete exchange of Na^+ and Fe^{3+}. Finally, the brown precipitate was collected and washed with methanol for several times and dried in oven at 60 °C for 2 h to remove remnant solvents. For silver oleate, the procedure is similar, where 12 mmol (4 ml) oleic acid and 12 mmol NaOH were needed for 12 mmol $AgNO_3$.

Synthesis of Ag/Fe_3O_4 composites

The composites were synthesized by one-step solvothermal reaction. In a typical procedure, silver oleate (0.25 mmol, 0.0973 g) and iron oleate (0.05 mmol, 0.0450 g) were dissolved in 30 ml octadecylene with stir and heating at 80 °C for 2 h and during this process, 0.5 ml oleic acid was injected as surfactant. Finally, the mixed solution was quickly transferred to a 50 ml Teflon-lined stainless steel autoclave and heated at 150 °C in an oven for 5 h. After the autoclave was cooled down to room temperature naturally, the black precipitate was with mixed solvent of hexane and isopropanol (volume ratio 1:4) for 4 times. Then the precipitate was washed with acetone for 2 times to remove remaining hexane. In the reaction system, the total dosage of silver oleate and iron oleate was fixed at 0.3 mmol. To make a comprehensive study, samples with various Ag/Fe molar ratios of 5, 2 and 1 were prepared, respectively. Ag NPs were synthesized as a control sample under the identical conditions but without the addition of iron oleate. Before SERS measurements, the precipitates were re-dispersed in 50 ml ethanol by sonication for 10 min.

Preparation of SERS substrates

Rhodamine 6G (R6G) and methyl blue (MB) dyes with various concentrations were used as analytes for SERS measurements. An external magnet was used to attract and transfer the nanocomposites of Ag/Fe_3O_4 to the surface of a 5 mm × 5 mm silicon slice. After the SERS substrate was dried at room temperature, it would be further tested by Raman instrument. The sample of naturally dispersed Ag NPs (Fe/Ag=0) was used to prepare referenced SERS substrate. To make a reasonable

comparison, the Ag NPs colloidal solution mixed with R6G or MB dye was firstly concentrated by the aid of centrifugal machine with a low rotation rate (5000 rpm) for 5 min, and then most of the liquid supernatant was removed. After the left slurry was ultrasonic dispersed again, certain amount (10 μL) of the mixture was dropped on the silicon substrate to fulfil the preparation of referenced SERS substrate.

Results and discussions

Fig. 1a shows the X-ray diffraction (XRD) patterns of samples with different Ag/Fe mole ratios. All of the diffraction peaks are well matched with the standard diffraction lines (PDF # 04-0783) of Ag-3C. Thus only cubic silver with space group of Fm-3m could be indexed. It is obvious that the peak intensity and full-width at half maximum (FWHM) become strong and narrowed respectively accompanied by increasing the mole ratios of Ag/Fe from 1:1 to 5:1. No detectable diffraction peaks of Fe_3O_4 are observed even in the sample of Ag/Fe = 1:1. However, although XRD is a powerful tool to well disclose the average period structure of crystals, the characteristic peaks for substance with badly poor crystallinity would be still concealed in the background. Therefore, a highly sensitive and ultra trace analysis technique—X-ray photoelectron spectroscopy (XPS)—was further applied to reveal the bonding and valence state of as-obtained composites. Fig. 1b shows the XPS peaks of Ag $3d_{3/2}$ and $3d_{5/2}$ with binding energies centered at 374.3 and 368.3 eV, respectively, which are assigned to metallic silver.[40, 41] The peaks of Fe $2p_{3/2}$ and Fe $2p_{1/2}$ shown in Fig. 1c are centered at 710.9 eV and 724.4 eV, close to the standard data of Fe_3O_4.[42] By deconvoluting Fe $2p_{3/2}$ peak into Fe^{2+} and Fe^{3+} (peaks at 710.50 eV and 712.15 eV, respectively), we calculate the integrated areas of Fe^{2+} and Fe^{3+}, and the corresponding values are listed in Table S1. The Fe^{2+}/Fe^{3+} molar ratio is 0.33:0.67, in accordance with that of Fe_3O_4 within the uncertainty of calculations. The satellite peak situated around 719 eV is a characteristic peak of Fe^{3+} in γ-Fe_2O_3, suggesting that Fe_3O_4 nanoparticles are partly oxidized. O 1s XPS peaks in Fig. 1d also match very well with that of the reported Fe_3O_4 standard samples.[42] Above all, XRD and XPS results verify that the as-prepared samples are composites of Ag and Fe_3O_4.

In this work, the low-temperature solvothermal reaction (150 °C) instead of high-temperature pyrolysis (usually >300 °C)[43] has been applied to fulfill the dissociation of iron oleate precursors, and as a result, the obtained Fe_3O_4 NPs deliver a attenuate size and crystallinity. TEM was used to afford more visualized proof of Ag/Fe_3O_4 composition by exposing the microstructure of Ag and Fe_3O_4. Fig. 2a shows that the size of Ag NPs without composited with Fe_3O_4 distributes from 10 nm to 30 nm. For sample of Ag/Fe = 5, the morphology and size of Ag NPs has no obvious change (Fig. 2b), but a gelatinous membrane emerges to link the Ag NPs together. The polycrystalline rings observed in the selected area diffraction (SEAD) pattern (Fig. 2c) are in good agreement with the face-centered cubic phase of Fe_3O_4 and Ag, revealing the nanocrystalline feature of Ag/Fe_3O_4 composites in the

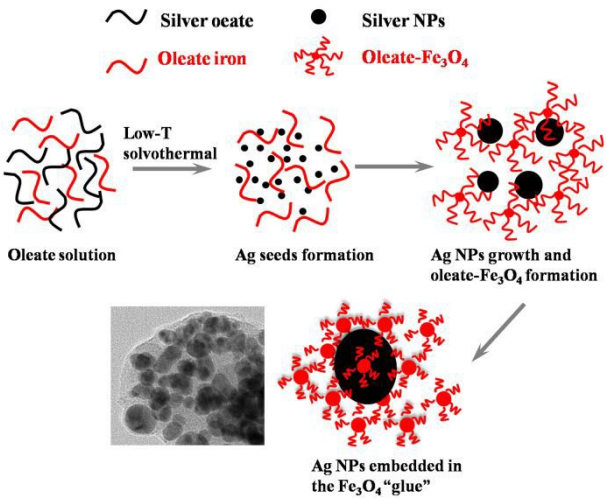

Scheme 1. The possible formation mechanism for the unique structure of Ag NPs attached to the "glue-like" Fe_3O_4 colloids.

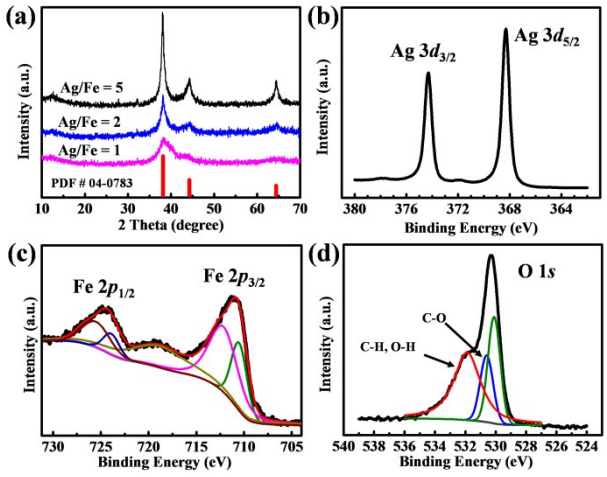

Fig. 1. (a) X-ray diffraction (XRD) patterns of as prepared Ag/Fe_3O_4 nanocomposite with variable Ag/Fe atoms ratio. The vertical red lines indicate the standard silver-3C diffraction lines (PDF # 04-0783). (b-d) XPS spectra of Ag 3*d*, O 1*s* and Fe 2*p* for the sample of Ag/Fe=5.

selected area. However, as demonstrated in HRTEM image (Fig 2d), most of the lattice fringes can be ascribed to Ag nanocrystals while the spacing of adjacent fringes 0.235 and 0.203 nm are corresponding to the (111) and (200) planes of Ag, respectively. Only a few tiny nanocrystals surrounded by the Ag NPs can be indexed to Fe_3O_4. In order to better analyze the component and microstructure of the glue-like membrane mentioned above, the sample of Ag/Fe = 1 was also characterized by TEM and HRTEM in Fig. 2e and 2f. Remarkably, the gelatinous component increases with the increase of Fe_3O_4 content. Most of the fringes of nanocrystals can be labeled as characteristic lattice plane of Fe_3O_4, as shown in HRTEM image of the glue-like area. Therefore, the glue-like membranes existing in Fig. 2b and 2e are mainly

constituted by Fe_3O_4 nanocrystals. As we can see, the glutinous Fe_3O_4 membranes here are just like "glue" that gum Ag NPs together.

The unique structure could be attributed to the difference of pyrolysis property between iron oleate and silver oleate. Just as depicted in Scheme 1, under a relatively low solvothermal reaction temperature (150 °C), silver seeds would be firstly formed by the decomposition of silver oleate precursors. Then the crystallite growth of Ag NPs is in consistent with the "Ostwald ripening", where the higher surface-free energy of small crystallites makes them less stable than larger crystallites and consequently dissolute in the solvent. The net result of this stability gradient is a slow diffusion of material from the surfaces of small particles to the surfaces of larger particles. The growth by this kind of transport can result in the poly-dispersed distribution of Ag NPs.[44]

However, it is more complex for iron oleate precursors. Jongnam Park et al.[43] have demonstrated that for solid iron oleate precursor, one oleate ligand first dissociates from the precursor at a relative low temperature (200-240 °C) and the remaining two oleate ligands dissociate at a higher temperature (~300 °C). Nucleation is triggered by the dissociation of one oleate ligand from the $Fe(oleate)_3$ precursor, while the major growth occurs at higher temperature initiated by the dissociation of the remaining two oleate ligands from the iron-oleate species. In addition, slow growth can also occur at <250 °C. In our work, the dissociation temperature of iron oleate is proved to be much lower in the high-pressure solvothermal reaction system. But only a slow growth can occur companied by the incomplete dissociation of oleate ligands and the formation of tiny oleate-Fe_3O_4 colloids. These tiny oleate-Fe_3O_4 NPs (in several nanometers) would finally cross-link together through the oleate ligands and become Fe_3O_4 magnetic "glue" around the Ag NPs. Under the action of the external magnetic field, the magnetized colloidal particles would drive the Ag NPs aggregated, just like the magnetic glue to stick the Ag NPs together.

Fig. 3 shows the UV-vis-NIR absorbance spectra of Ag/Fe_3O_4 nanocomposites with different Ag/Fe molar ratios. Ag NPs derived from silver oleate precursors via solvothermal reaction possess intense SPR absorption peak centered at 425 nm. Once compounded with Fe_3O_4, the SPR peaks are obviously suppressed. The peaks for Ag/Fe = 5, Ag/Fe = 2, Ag/Fe = 1 are located around 430, 433, 437 nm, respectively. It is noted that by adding more ferric precursors in the reaction system, the absorption peaks gradually shift towards the long wavelength, which is probably due to the multi-nanoparticles aggregation induced by gelatinous Fe_3O_4.

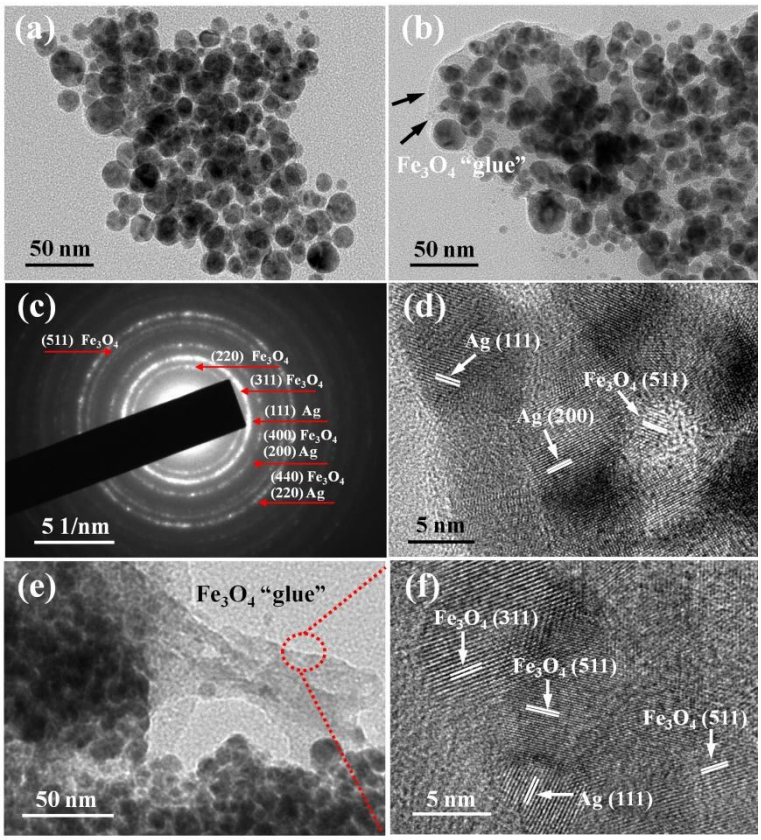

Fig. 2 (a) TEM image of Ag NPs without composited with Fe_3O_4. (b-d) TEM, selected area electron diffraction (SAED), and high-resolution TEM (HRTEM) images for sample of Ag/Fe=5. (e-f) TEM and HRTEM images for sample of Ag/Fe=1.

RSC Advances

ARTICLE

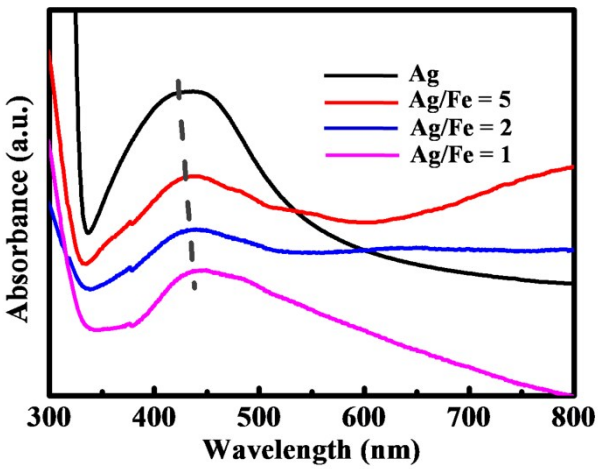

Fig. 3 UV-vis-NIR absorbance spectra of Ag/Fe_3O_4 nano-composites with different Ag/Fe molar ratios.

Magnetic properties of the as-synthesized Ag/Fe_3O_4 nanocomposites were further characterized by VSM at room temperature. Fig. 4 presents the magnetic hysteresis loops of samples with Ag/Fe = 5, Ag/Fe = 2 and Ag/Fe = 1. The saturation magnetization (M_s) of Ag/Fe_3O_4 nanocomposites are 6.62, 13.60 and 24.72 emu/g respectively for Ag/Fe = 5, Ag/Fe = 2, and Ag/Fe = 1. Fig. S1 (see the magnified low field curves in supporting information) further reveals that the as-prepared Fe_3O_4 NPs in composites possess excellent superparamagnetic performance as the remnant magnetization (M_r) and coercivity (H_c) are very close to zero. A good magnetic responsivity of these nanocomposites can be also exposed by the fact that they are quietly apt to be attracted by an external magnet. The inserted digital photographs in Fig. 4 indicate that even for sample of Ag/Fe = 5 with saturation magnetization as low as 6.62 emu/g, the nanocomposites dispersed in ethanol would be quickly attracted to the glass wall leaving the ethanol solution transparent when a permanent magnet of NdFeB is placed closed to the vial. Once the magnet is removed, the nanocomposites of Ag/Fe_3O_4 could be well dispersed again by hand-rocking the vial for several times.

It is well-known that the aggregation of noble metal is conducive to introduce more "hot spots" located at intermediate gaps between metal NPs. Herein, the magnetism induced aggregation can be utilized to realize superior SERS behavior. Fig. 5a shows the spectra of R6G collected on samples of Ag NPs, Ag/Fe = 2 and Ag/Fe = 5. Peaks centered at 1184, 1312, 1367, 1508, and 1653 cm^{-1} are assigned to the vibrations of C-H in-plane bending, C-O-C stretching, and C-C stretching of the aromatic ring.[45, 46] Besides, peak centered at 613 and 778 cm^{-1} corresponds to the in-plane deformation vibration of the ring and out-of-plane bending motion of the hydrogen atoms of xanthenes skeleton, respectively.[22, 32] In order to convictively evaluate the SERS activity of composite substrates of Ag/Fe_3O_4 with different Ag/Fe ratios, the SERS property of naturally dispersed Ag NPs without Fe_3O_4 was also investigated. It is explicit that both composite samples deliver largely enhanced SERS activity compared with the natural dispersed Ag NPs. Usually, the improved SERS activity is ascribed to more probe molecules adsorbed on Ag/Fe_3O_4 aggregates as well as the increased "hot spots" derived from magnetism-induced aggregation of Ag NPs. In addition, the substrate of Ag/Fe = 5 displays the strongest SERS signals compared with that of Ag/Fe = 2 and Ag NPs. For the typical band at 1367 cm^{-1}, the relative enhancement factor (EF) for Ag/Fe_3O_4 = 5 reaches up to ~10^2 compared with the naturally dispersed Ag NPs. MB, another typical dye with a large Raman scattering cross section, is also introduced to evaluate the SERS activity of Ag, Ag/Fe = 5 and Ag/Fe = 2 (Fig. 5b). The characteristic peak at around 1618 cm^{-1} ascribed to the C–C stretching of MB molecular is adopted to estimate the SERS property of hybrid substrate. The sample of Ag/Fe = 5 still exhibits the best SERS activity and the corresponding spectra is enhanced by up to~20 times than that of naturally dispersed Ag NPs. Therefore, by this facile one-pot solvothermal method, the as-prepared Fe_3O_4/Ag composite substrates shows greatly improved SERS performance due to the external magnet induced self-aggregation of Ag NPs.

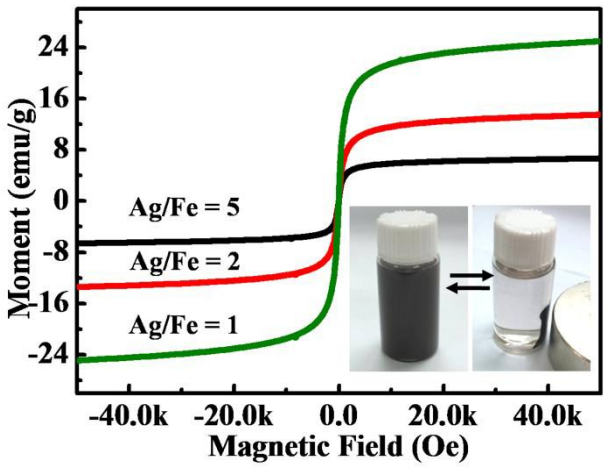

Fig.4 Magnetic hysteresis loops of the composites of Ag and Fe_3O_4 with different Ag/Fe molar ratios. The inserts are photographs of sample with Ag/Fe = 5 taken before and after magnetic separation by an external magnet.

The effect of the external magnetic field intensity on the SERS activity of our substrates is also studied. A qualitative alteration for the magnetic field is conducted by adjusting the distance (*d*) between the sample and the permanent magnet (Fig. S2a). After fixing the positions of glass slide and magnet, 25 μl well-dispersed colloid solution was dropped on the slide, and all the samples were naturally dried at the ambient temperature. Fig. S2b shows the SERS spectra collected on the sample of Ag/Fe=5 with different *d* values. The spectrum collected without the aid of magnet is also given for reference. There is no obvious difference between the spectra collected at *d*=0 and *d*=2 cm, but the intensity of Raman bands clearly decreases with *d*=6 cm. Without the magnet, the integrated intensity for the band at 612 cm^{-1} largely degreases by 52% in comparison with that of the spectrum collected with *d*=0 cm. When the external magnetic field is below the saturation value, the larger of the magnetic field, the more effective "hot spots" will appear. However, there is no much influence on the SERS activity for the magnetic field intensity when the magnetic field is above the saturation one.

To further illustrate the enhancement mechanism of glue-like Fe_3O_4 for the improved SERS activity of Ag/Fe_3O_4 composite substrate, a schematic diagram based on Fig. S3a was presented in Fig. S3b. Under the action of an external magnetic field, the glue-like Fe_3O_4 colloids with good superparamagnetism would be magnetized easily, and simultaneously the Ag NPs adhering to the Fe_3O_4 "glue" are driven to aggregate together. Besides, the aggregated composite substrate could also increase the density of the adsorbed analyte molecules. So Fe_3O_4 "glue" here serves as a contractile net to collect Ag NPs and analyte molecules together, which would lead to highly dense and intense "hot-spots". However, excess Fe_3O_4 "glue" component in the composite substrate would weaken the SERS activity, which has been confirmed by the fact that the substrate with Ag/Fe = 2 shows sharply declined SERS activity compared with the substrate with Ag/Fe = 5. To make it easier to understand, a schematic diagram is shown in Scheme S1 (Supporting Information). For the substrate of Ag/Fe = 5, the Ag NPs are driven to aggregate effectively by the magnetized Fe_3O_4 "glue" and thereby plenty of "hot-spots" located at the sub-10 nm gaps are built. The concentration of the Fe_3O_4 colloidal NPs for Ag/Fe = 2 is theoretical 2 times larger than that for Ag/Fe = 5, and therefore the Fe_3O_4 "glue" around Ag NPs is much thicker in Ag/Fe = 2. It should be noted that the Fe_3O_4 species hardly show any SERS activity, and excess Fe_3O_4 component do not contribute to the SERS performance. Within a laser spot volume, there are less Ag NPs as well as "hot-spots" for Ag/Fe = 2 as the magnetic "glue" component in Ag/Fe = 2 has occupied too much space. In fact, more magnetic "glue" component does not mean more "hot-spots" for Ag NPs, which is because the Ag NPs concentration could be greatly diluted by too much Fe_3O_4 "glue". The as-prepared composite substrates of Ag/Fe_3O_4 = 5, which consists of low Fe_3O_4 content but with excellent superparamagnetism, have exhibited more outstanding SERS properties than the reported ones with higher content and larger-sized Fe_3O_4.[32]

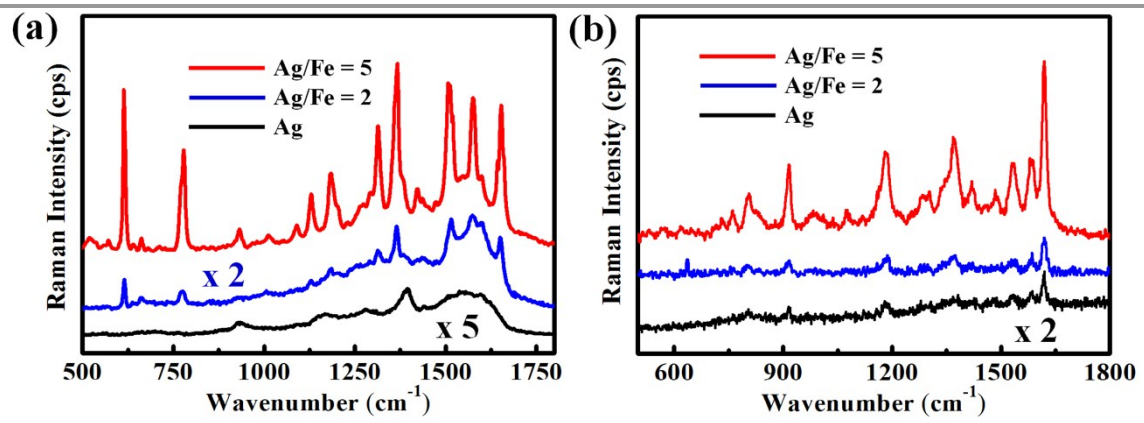

Fig. 5 (a) SERS spectra of R6G collected on samples of Ag, Ag/Fe = 5 and Ag/Fe = 2. R6G concentration, 10^{-9} M; For better comparison, the intensity for Ag/Fe = 2 and Ag are multiplied by 2 and 5, respectively. (b) SERS spectra of MB collected on samples of Ag, Ag/Fe = 5 and Ag/Fe = 2. MB concentration: 10^{-8} M; For better comparison, the intensity for Ag is multiplied by 2.

RSC Advances

ARTICLE

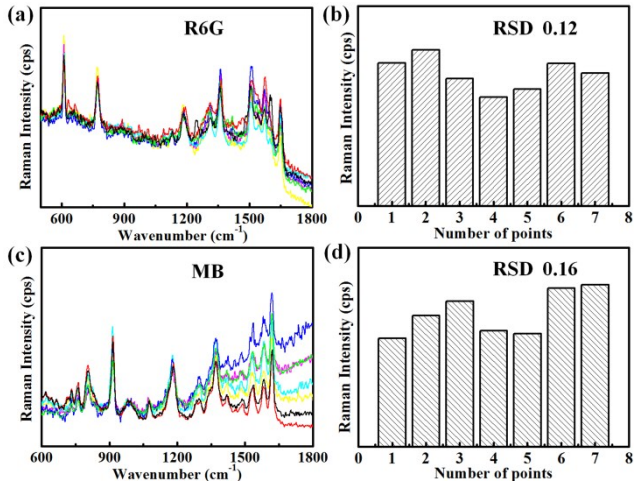

Fig. 6 (a) A series of SERS spectra of R6G molecules collected from two arbitrary Ag/Fe = 5 substrates and (b) the corresponding integrated intensity of the main peak at 612 cm^{-1} for R6G molecules collected at 7 different points. The calculated relative standard deviation (RSD) value is 0.12. (c) Raman spectra of MB molecules collected from two arbitrary Ag/Fe = 5 substrates and (d) the corresponding integrated intensity of peak at 913 cm^{-1}, which give a RSD value of 0.16.

In literature, the enhancement factor (EF) provides an important aspect of the SERS substrate performance compared with various SERS substrate. To estimate the SERS enhancement, we calculate the EF value by the formula as followed:

$$EF=\left(\frac{I_{SERS}}{I_{Raman}}\right)\left(\frac{N_{Raman}}{N_{SERS}}\right)$$

I_{SERS} and I_{Raman} refer to the integrated intensity of Raman peaks corresponding to the same vibration mode in the SERS spectrum and Raman spectrum of bulk dyes (R6G and MB). N_{SERS} and N_{Raman} are the number of adsorbed dye molecules to the SERS active substrate and solid dye molecules both in a laser spot volume. For N_{Raman} calculation, the spectra of solid R6G and MB are used. The detailed calculation method is given in supporting Information. The calculated Raman EFs deduced from Fig. S4 are 1.58×10^8 and 1.46×10^8 for R6G, MB detection respectively on composite SERS substrate with Ag/Fe = 5. The large EFs, which are mainly attributed to the increased "hot spots" generated by magnetic glue-like Fe_3O_4 NPs induced aggregation of Ag NPs, about 1~2 orders of magnitude more than the reported results for the core-shell structure prepared by a general two-step method.[47]

Additionally, the signal reproducibility is another concern to evaluate the effective SERS substrate in practical applications. Fig. 6 shows the SERS spectra of R6G and MB respectively collected from two arbitrary samples under the same experimental conditions. The relative standard deviation (RSD) of major peaks is often used to estimate the reproducibility of experiment. Both the RSD values are below 0.2 for the main peaks located at 612 cm^{-1} for R6G molecules and 913 cm^{-1} for MB molecules, which demonstrates the as-prepared Ag/Fe_3O_4 composite substrates are relatively homogeneous and stable.

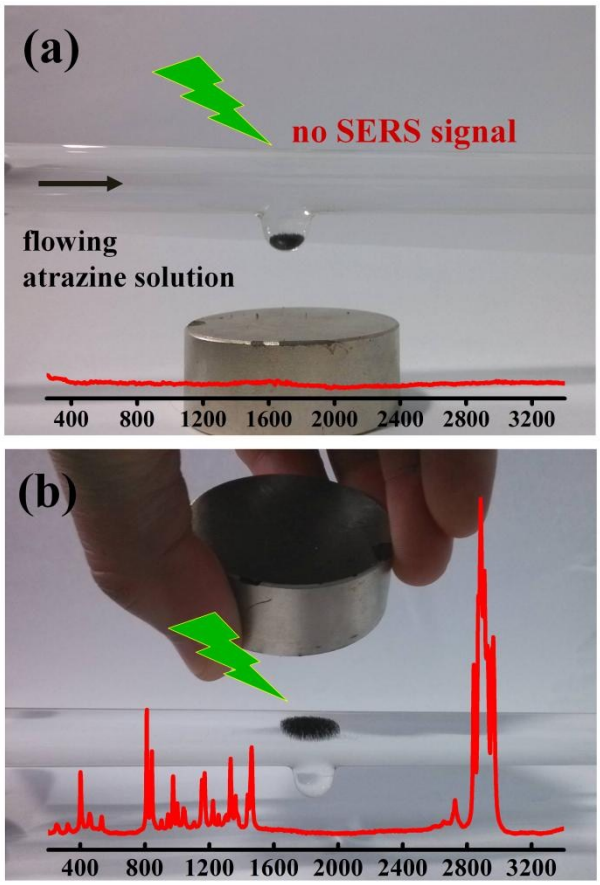

Fig. 7 Real-time on-line monitoring of flowing atrazine solution (10^{-6} M). (a) Ag/Fe_3O_4 nanocomposite are magnetic attracted and stored in the tank cell, and under this mode no SERS signals were detected. (b) Ag/Fe_3O_4 nanocomposite was magnetic attracted to the pipe wall to turn on real-time on-line monitoring mode, and greatly enhanced SERS signals of atrazine were obtained.

An efficient real-time on-line monitoring system is in urgent need for the monitoring of sewage discharge in food and medicine production, which are inextricably bound to the life of human beings. SERS technology is one of the most

promising methods to realize ultra-fast, high sensitive, real-time on-line monitoring. However, to our best knowledge, there have been few studies on the on-line monitoring of contaminated water by use of the SERS technology, which is probably due to the lack of flexible and controlled SERS substrate. Here, by strategically utilizing the bifunctional Ag/Fe_3O_4 composites SERS substrates, we designed a smart real-time on-line monitoring system. Just as shown in Fig. 7, the flowing atrazine aqueous solution with a concentration of 10^{-6} M in a quartz tube was adopted to simulate the waste water contaminated by pesticide. Atrazine, one kind of the most commonly used herbicide in China, US and probably the world, has been not only threatening the surface and ground water, but damaging the immune system and endocrine system of living organisms. Seen from the molecular structure in Scheme S2, atrazine has the binding sites of N⋯Ag molecular complexes. Before collecting the SERS signals, the Ag/Fe_3O_4 composite substrate is stored in the tank cell for several minutes to reach the maximum adsorption of atrazine molecules. The shell of the quartz tube is ~1 mm in thick and transparent for the 532 nm laser, so the laser beam would penetrate the shell and reach the composite SERS substrate once the substrate is transferred to the detection site by external magnet.

Fig. 7a indicates that under the "turn-off" mode, the magnetic nanocomposites are stored in the tank cell by an external magnet, and no detectable Raman signal of atrazine could be observed. Once turning on the real-time on-line monitoring mode by attracting the nanocomposites to the pipe wall (at laser focal point), greatly enhanced SERS signals of atrazine can be obtained as presented in Fig. 7b. These characteristic Raman peaks are in good agreement with that of atrazine reported in literature.[48] It is noteworthy that the maximum allowable concentration of atrazine is imposed to be below 3 mg/L (13.9 μmol/L) according to the effluent standards of pollutants for heterocyclic pesticides industry (GB21523-2008) in China. Surely, our designed system based on the magnetic Ag/Fe_3O_4 composite is perfectly able to fulfill the effective real-time on-line monitoring of atrazine contaminated water.

The magnetism-controlled SERS on-line monitoring device was further used to detect the irrigating water in the suburbs of Shanghai. Two water samples were collected from a ditch in the corn fields and the underground water respectively. The Raman spectrum shown in Fig. 8a indicates there is no detectable pollutant in the irrigating water from the underground, while Fig. 8b reveals that the water in the ditch has been contaminated by atrazine as several characteristic Raman peaks of atrazine have been detected. Therefore, the magnetism-controlled on-line monitoring system based on our Ag/Fe_3O_4 composite SERS substrate here can be also popularized to many other fields, which is a promising strategy to accomplish an efficient and convenient on-line monitoring in industrial or agricultural production.

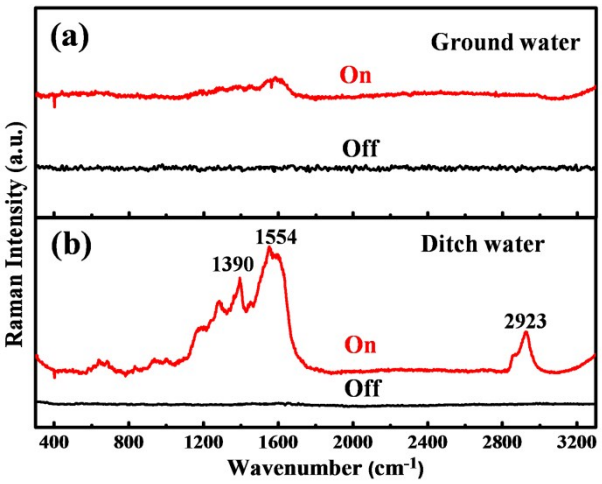

Fig. 8 (a) SERS spectra of untainted irrigating water measured by the on-line monitoring system. (b) Characteristic Raman peaks of atrazine were detected by the same monitoring system from atrazine contaminated water drawn from the ditch. "On" mode means to turn on the on-line monitoring while "Off" mode means to turn off the on-line monitoring.

Conclusions

In summary, Ag/Fe_3O_4 nanocomposites have been obtained via a facile and efficient one-pot solvothermal method by using metal fatty acid salts as precursors. Ultra small Fe_3O_4 NPs that wrap Ag nanocrystals together just act as "glue" or contractile "net". The Fe_3O_4 NPs possess excellent superparamagnetic property that has been verified by the magnetic hysteresis loops, which could bring a profitable aggregation of Ag NPs under the action of external magnet. The SERS results for both R6G and MB molecules detection indicate that the samples of Ag/Fe = 5 show the most excellent SERS activity compared with Ag/Fe =2 and naturally dispersed Ag NPs. Low content of Fe_3O_4 but with prominent magnetic property can effectively make an aggregation of Ag NPs by an external magnet. The enhancement factors (EFs) of Ag/Fe = 5 for R6G and MB detection are over 1×10^8, which is superior to that of many reported core-shell composite of Ag/Fe_3O_4. Meantime, the as-prepared SERS substrates also show good reproducibility. Accordingly, this facile one-pot solvothermal method is certified to be an effective strategy to prepare highly active composite SERS substrates. The as-prepared Ag/Fe_3O_4 nanocomposites have been proved to be capable to real-time on-line monitor the atrazine molecules in the flowing solution which shows great potential for future applications in on-line monitoring of industrial or agricultural production.

Acknowledgements

This study was supported by a fund from the National Natural Science Foundation of China (No. 51471182).

Notes and references

§ In china, farmers just planted the spring corn at the end of April in the suburbs of Shanghai, and before the germination, atrazine was chosen to get rid of the weeds. They drew the water from a small ditch near the corn fields to dissolve the atrazine contained pesticides. In the meantime, the ditch was unavoidably polluted as the bottles and packing bags of pesticide were abandoned in the ditch, and the farmers also washed their sprayers with the ditch water. We took a water sample from this ditch, and to make a comprehensive comparison, we also collected another water sample drew from underground in greenhouse. The two water samples were directly poured into the as-designed on-line monitoring pipe respectively and the corresponding analysis results are shown in Fig. 8.

1 Y. Cao, D. Li, F. Jiang, Y. Yang, and Z. Huang, *J. Nanomater.*, 2013, **2013**, 12
2 Y. Shan, Y. Yang, Y. Cao, H. Yin, N. V. Long and Z. Huang, *RSC Adv.*, 2015, **5**, 34737-34743
3 M. Fleischmann, P. J. Hendra and A. J. McQuillan, *Chem. Phys. Lett.*, 1974, **26**, 163-166.
4 Y. Yang, Z.-Y. Li, K. Yamaguchi, M. Tanemura, Z. Huang, D. Jiang, Y. Chen, F. Zhou and M. Nogami, *Nanoscale*, 2012, **4**, 2663-2669.
5 D. Qi, L. Lu, L. Wang and J. Zhang, *J. Am. Chem. Soc.*, 2014, **136**, 9886-9889.
6 J. Ni, R. J. Lipert, G. B. Dawson and M. D. Porter, *Anal. Chem.*, 1999, **71**, 4903-4908.
7 X. Qian, J. Li and S. Nie, *J. Am. Chem. Soc.*, 2009, **131**, 7540-7541.
8 W.-H. Hsiao, H.-Y. Chen, Y.-C. Yang, Y.-L. Chen, C.-Y. Lee and H.-T. Chiu, *Acs Appl. Mater. Inter.*, 2011, **3**, 3280-3284.
9 Y. Yang, M. Tanemura, Z. Huang, D. Jiang, Z.-Y. Li, Y.-p. Huang, G. Kawamura, K. Yamaguchi and M. Nogami, *Nanotechnology*, 2010, **21,** 325701.
10 Y. Yang, J. Shi, T. Tanaka and M. Nogami, *Langmuir*, 2007, **23**, 12042-12047.
11 B. Han, N. Choi, K. H. Kim, D. W. Lim and J. Choo, *J. Phys. Chem. C*, 2011, **115**, 6290-6296.
12 A. M. Schwartzberg, C. D. Grant, A. Wolcott, C. E. Talley, T. R. Huser, R. Bogomolni and J. Z. Zhang, *J. Phys. Chem. B*, 2004, **108**, 19191-19197.
13 L. Zhang, W.-F. Dong, Z.-Y. Tang, J.-F. Song, H. Xia and H.-B. Sun, *Opt. Lett.*, 2010, **35**, 3297-3299.
14 N. R. Yaffe and E. W. Blanch, *Vib. Spectrosc.*, 2008, **48**, 196-201.
15 M. G. Espinoza, M. L. Hinks, A. M. Mendoza, D. P. Pullman and K. I. Peterson, *J. Phys. Chem. C*, 2012, **116**, 8305-8313.
16 X. Dong, H. Gu and F. Liu, Spectrochim. Acta A, 2012, **88**, 97-101.
17 L. Yang, H. Liu, J. Wang, F. Zhou, Z. Tian and J. Liu, *Chem. Commun.*, 2011, **47**, 3583-3585.
18 A. F. Chrimes, K. Khoshmanesh, P. R. Stoddart, A. A. Kayani, A. Mitchell, H. Daima, V. Bansal and K. Kalantar-zadeh, *Anal. Chem.*, 2012, **84**, 4029-4035.
19 L. Sun, J. He, S. An, J. Zhang and D. Ren, *J. Mol. Struct.*, 2013, **1046**, 74-81.
20 J. Du and C. Jing, *J. Phys. Chem. C*, 2011, **115**, 17829-17835.
21 S. Guo, S. Dong and E. Wang, *Chem.- Eur. J.*, 2009, **15**, 2416-2424.
22 Z. Gan, A. Zhao, M. Zhang, D. Wang, H. Guo, W. Tao, Q. Gao, R. Mao and E. Liu, *J. Nanopart. Res.*, 2013, **15** (11), 1-12
23 J. Bao, W. Chen, T. Liu, Y. Zhu, P. Jin, L. Wang, J. Liu, Y. Wei and Y. Li, *Acs Nano*, 2007, **1**, 293-298.
24 H.-L. Sun, M.-M. Xu, Q.-H. Guo, Y.-X. Yuan, L.-M. Shen, R.-A. Gu and J.-L. Yao, *Spectrochim. Acta A*, 2013, **114**, 579-585.
25 Y. Hu and Y. Sun, *J. Phys. Chem. C*, 2012, **116**, 13329-13335.
26 M. Chen, Y. N. Kim, H. M. Lee, C. Li and S. O. Cho, *J. Phys. Chem. C*, 2008, **112**, 8870-8874.
27 H. W. Gu, Z. M. Yang, J. H. Gao, C. K. Chang, B. Xu, *J. Am. Chem. Soc.* 2005, **127**, 34-35.
28 J. Du and C. Jing, *J. Colloid Interf. Sci.*, 2011, **358**, 54-61.
29 J. Huang, Y. Sun, S. Huang, K. Yu, Q. Zhao, F. Peng, H. Yu, H. Wang and J. Yang, *J. Mater. Chem.*, 2011, **21**, 17930-17937.
30 Q. An, P. Zhang, J.-M. Li, W.-F. Ma, J. Guo, J. Hu and C.-C Wang, *Nanoscale*, 2012, **4**, 5210-5216.
31 Y. Wang, K. Wang, B. Zou, T. Gao, X. Zhang, Z. Du and S. Zhou *J. Mater. Chem. C*, 2013, **1**, 2441-2447.
32 H. Guo, A. Zhao, Q. Gao, D. Li, M. Zhang, Z. Gan, D. Wang, W. Tao and X. Chen, *J. Nanopart. Res.*, 2014, **16**, (8), 1-8.
33 W. Yu, Y. Huang, L. Pei, Y. Fan, X. Wang and K. Lai, *J. Nanomater.*, 2014, **6** (17), 7083-7087
34 X. Zhang, C. Niu, Y. Wang, S. Zhou and J. Liu, *Nanoscale*, 2014, **6**, 12618-12625.
35 C. Yuen and Q. Liu, *Colloidal Nanopart. Biomed. App. IX*, 2014, 895516.
36 J. Du, J. Cui and C. Jing, *Chem. Commun.*, 2014, **50**, 347-349.
37 Q. Gao, A. Zhao, Z. Gan, W. Tao, D. Li, M. Zhang, H. Guo, Wang, H. Sun, R. Mao and E. Liu, *Crystengcomm.*, 2012, **14**, 4834-4842.
38 S. Zhu, C. Fan, J. Wang, J. He, E. Liang and M. Chao, *J. Colloid Interf. Sci.* 2015, **438**, 116-121.
39 N. R. Jana, Y. Chen and X. Peng, *Chem. Mater.*, 2004, **16**, 3931-3935.
40 M.-J. Kim, H.-J. Na, K. C. Lee, E. A. Yoo and M. Lee, *J. Mater. Chem.*, 2003, **13**, 1789-1792.
41 Q. Zhang, J. Li, X. Liu and Q. Zhu, *Appl. Catal. A-Gen.*, 2000, **197**, 221-228.
42 T. Yamashita and P. Hayes, *Appl. Surf. Sci.*, 2008, **254**, 2441-2449.
43 J. Park, K. An, Y. Hwang, J.-G. Park, H.-J. Noh, J.-Y. Kim, J.-H Park, N.-M. Hwang and T. Hyeon, *Nat. mater.*, 2004, **3**, 891-895.
44 D. K. Lee, Y. S. Kang, ETRI J., 2004, **26** (3), 352-256.
45 M. Zhang, A. Zhao, H. Guo, D. Wang, Z. Gan, H. Sun, D. Li and M. Li, *Crystengcomm.*, 2011, **13**, 5709-5717.
46 L. Sun, Y. Song, L. Wang, C. Guo, Y. Sun, Z. Liu and Z. Li, *J. Phys. Chem. C*, 2008, **112**, 1415-1422.
47 Z. Y. Bao, J. Dai, D. Y. Lei and Y. Wu, *J. Appl. Phys.*, 2013, **114**, 124305.
48 S. Bonora, E. Benassi, A. Maris, V. Tugnoli, S. Ottani and M. Di Foggia, *J. Mol. Struct.*, 2013, **1040**, 139-148.

TOC

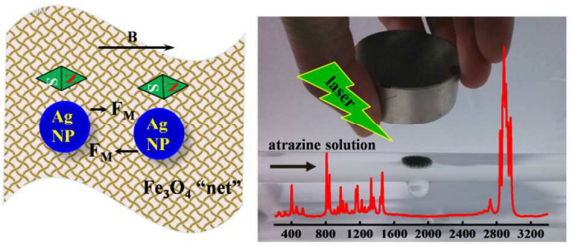

The dual-functional substrates of Ag/Fe_3O_4 exhibit excellent SERS performance, and have been successfully applied in real-time on-line monitoring of wastewater.